Latin American Journal of Solids and Structures
www.lajss.org

Multiscale Failure Analysis of Cylindrical Composite Pressure Vessel: A Parametric Study

Abstract
This paper deals with a multiscale approach to model thick-walled laminate cylinder with internal pressure. Micromechanics defines material homogenization considering two steps: determination of equivalent properties of each lamina from matrix and fiber properties according to the Mori-Tanaka model for elastic properties and to the Bridging model for strengths; and determination of anisotropic homogeneous properties of the laminate built with a set of laminae using asymptotic homogenization. On the other hand, macromechanics determines stress and failure analysis. Lekhnitskii formalism is used to obtain the elastic solution of the stress and strain distributions and failure is analyzed employing the Tsai-Wu criterion. Three different pressure vessel configurations are analyzed according to end conditions: restrained-ends, open-ends and closed-ends. Angle-ply laminates made of carbon fibers and epoxy matrix are considered to evaluate the influence of lay-up angle, fiber volume fraction, wall thickness and end-conditions. The optimum angles as well as the maximum internal pressure are obtained and a parametric analysis is presented. The main results indicate that the optimum angle is almost constant for restrained and closed-ends. On the other hand, for open-end, angle varies in a significant way. Besides, results show that the increase the fiber volume fraction is more effective to increase vessel strength than the increase of the number of layers.

Keywords
pressure vessel, homogenization, multiscale analysis.

Lucas Lisbôa Vignoli[a]*
Marcelo Amorim Savi[a]

[a] Centro de Mecânica Não-Linear - Departamento de Engenharia Mecânica - COPPE - Universidade Federal do Rio de Janeiro, Rio de Janeiro, RJ, Brasil. E-mail: ll.vignoli@mecanica.coppe.ufrj.br, savi@mecanica.ufrj.br

*Corresponding author

https://doi.org/10.1590/1679-78254323

Received: July 27, 2017
In Revised Form: December 08, 2017
Accepted: December 27, 2017
Available Online: February 05, 2018

1 INTRODUCTION

Structures made of composite materials have been widely used due to advantages related to joining materials with different properties, exploiting the best of each one of them. Anisotropy and heterogeneity are essential characteristics of composite materials that make their mechanical modeling hard and complex. Composite pressure vessels have been studied by different approaches during decades. It has been the objective of several research efforts by large industrial applications such as fluid storage and transportation. Despite this, there are still nowadays challenges related to several design issues, as failure criteria, mainly for 3D stress state (Kaddour and Hinton, 2013), and stress concentration modeling (Vignoli and Savi, 2017).

Lekhnitskii formalism constitutes one of the most used analytical approaches for three-dimensional solutions in anisotropic elasticity (Lekhnitskii, 1981). The major contributions of the elasticity based solutions are related to Ting (1996, 1999) and Chen *et al.* (2000). A complementary approach is presented by Evans and Gibson (2002), which studied the influence of the ratio of mechanical properties of fibers and matrix on failure mechanism.

Based on these theoretical advances, Tita *et al.* (2012) developed a computational tool to analyze thick laminate tubes subjected to internal pressure with a simplified homogenized solution. In an alternative way, Ansari *et al.* (2010) proposed a hybrid analytic-numerical solution based on the three-dimensional theory of elasticity and applying the finite difference method to solve the governing equations, obtaining stress and strain distributions through the laminate tube wall subjected to thermomechanical dynamical loads.

All these studies use anisotropic macromechanical properties. In this regard, mutiscale approach constitutes a design improvement, allowing one to consider the influence of constituents as well as laminate lay-up. Chatzigeorgiou *et al.* (2008) and Sun *et al.* (2014) explored the homogenization of layered tubes with interface abrupt

material property variations. The main advantage of the multiscale homogenization is that all the interface boundary conditions (*i.e.* force equilibrium and displacement continuity) are intrinsically satisfied, eliminating the necessity to solve a system of equations associated with a laminate composed by a set of concentric tubes, where each layer lamina is an independent structure. Another multiscale approach is presented by Liu *et al*. (2012) using finite element method. The influence of the pressure load in a homogenized pressure vessel considering damage of the representative volume element (RVE) is analyzed. According to Carrere *et al*. (2012a, 2012b), this multiscale approach is the most recommended design guideline.

Multiscale characteristics associate the composite structure optimization design to a large amount of variables including constituent volume fractions (Tsai and Melo, 2014). Experimental approach can be employed to deal with that, as presented in by Cohena *et al*. (2001), which reports that the strength of a graphite-epoxy filament wound tube increased around 10% if the fiber volume fraction is increased from 0.52 to 0.65. Rafiee and Amini (2015) pointed that the increase of the fiber volume fraction may result in a smaller failure pressure depending on the winding angle.

A review of pressure vessel design challenges are detailed by Martins *et al*. (2012, 2013, 2014) including the optimum winding angle according to the end-load condition and different failure modes. The authors classified the end-condition in three different ways: closed-ends, which is the most common pressure vessel application for fluid storage, and open and restrained-ends, which are usually applied to model pipeline conditions. The restrained-ends condition is equivalent to the plane strain hypothesis, being the objective of the analysis of Christensen (2005). Onder *et al*. (2009) also studied different failure mechanism for first ply failure (FPF) and burst of glass fiber closed-ends pressure vessels.

Additional contributions have been done by Drozdov and Kalamkarov (1995) that proposed an analytical model to evaluate the optimum preload during winding fabrication process of pressure vessels considering the layers as viscoelastic materials. An overview of manufacture issues can be found in Barbero (1998). Kam *et al*. (1997) and Chang (2000) presented experimental results of FPF pressure using acoustic emission technique for damage detection. Krikanov (2000) considered the influence of mass and stiffness for an optimization analysis. Parnas and Katırcı (2002) developed a procedure to study filament wound cylinders for motor applications where, additionally to the internal pressure, an axial force and a body force from angular velocity are considered. They concluded that the application of axial force decreases the optimum winding angle while the angular velocity tends to increase for values close to 90°. Quaresimin and Carraro (2014) investigated multiaxial fatigue effect in glass fiber laminate tubes. Sarvestani *et al*. (2016) proposed a method based on the layerwise theory to study laminate tubes subjected to bending and transverse shear loads. Almeida Jr. *et al*. (2016) proposed a computational approach for damage progression of composite tubes with external pressure loads.

This article deals with the design of pressure vessel considering the influence of end conditions, lay-up and fiber volume fraction on failure. A multiscale approach is adopted using micromechanics to define lamina properties and the equivalent laminate properties. Macromechanical analysis considers elasticity-based stress and strain distributions as well as failure criterion. Micromechanics employs Mori-Tanaka model to estimate elastic properties and the Bridging model to compute strengths of the lamina. Afterward, asymptotic homogenization is applied to transform the laminate in a homogenous anisotropic equivalent cylinder. On the other hand, macromechanics uses the Lekhnitskii formalism to obtain the stress and strain distributions. Strain components are used to define the failure according to the Tsai-Wu criterion. Carbon fiber and epoxy matrix are selected to study the maximum pressure and optimum angle in angle-ply laminates according to the end conditions, fiber volume fraction and vessel thickness through a parametric analysis.

2 MICROMECHANICS ANALYSIS

Several models have been proposed to estimate equivalent properties of the lamina from constituent data. Basically, this is established by micromechanics analysis related to analytical semi-empirical tools, elasticity-based models, homogenization models, among other possibilities. Nevertheless, the majority of models are related to elastic properties, being not able to predict strengths. The definition of stiffness and compliance tensors of a unidirectional lamina uses five independent elastic constants; on the other hand, failure analysis employs six strengths (Lekhnitskii, 1981; Kaddour and Hinton, 2012). A complete micromechanical model must be able to predict all of these eleven properties.

This work employs micromechanical models that are separated into two parts: initially, elastic properties are estimated using the Mori-Tanaka model and the strengths are predicted using the Bridging model for a single lamina; next, the asymptotic homogenization is applied to obtain the equivalent properties of the homogenized laminate considering an angle-ply lay-up $[\pm\alpha]_n$, where n is the number of repetition of the plies $+\alpha$ and $-\alpha$. The

Bridging model was first derived based on the Mori-Tanaka approach (Huang, 2000; Huang and Zhou, 2011) and later an alternative formulation using the three-phase model was proposed resulting in similar predictions (Wang and Huang, 2015).

Basically, all interfaces are assumed to be perfectly bonded. These interfaces include fiber-matrix and consecutive plies. Carneiro and Savi (2000) proposed an interface constitutive model describing delamination effects. Sevostianov *et al.* (2012) discussed different approaches to deal with imperfect interface modeling. Macedo *et al.* (2017) presented an alternative numerical methodology to evaluate mechanical behavior of unidirectional laminates based on the asymptotic homogenization theory including interface effects.

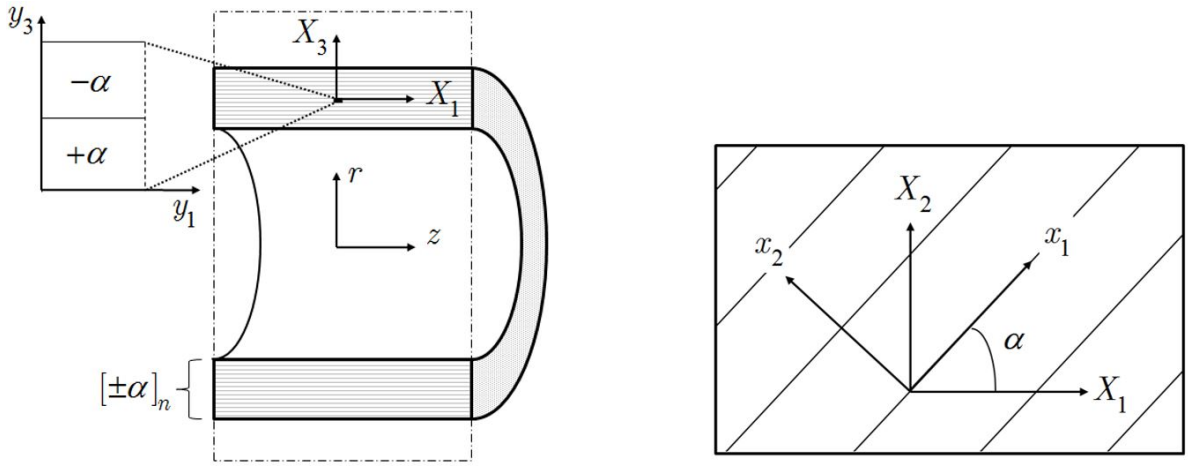

Figure 1: *Coordinate systems used at the pressure vessel modelling.*

Composite material description needs to proper establish the coordinate systems definition. Four different coordinate systems are necessary (see Fig.1): cylindrical coordinates, r, θ and z, used to describe the macroscopic aspects of the structure (i.e. stress and failure analysis); local coordinate, x_i, where x_1 coincides to the lamina fiber direction; global coordinate, X_i, used as reference to the homogenized properties and X_1, X_2 and X_3 coincides with the directions of z, θ and r, respectively; and micro-coordinate, y_i, used on the asymptotic homogenization process (section 2.2). Since the asymptotic homogenization is carried out on the radial direction, this is essentially one-dimensional being convenient to define $y_3 = X_3 / \varepsilon$, where $\varepsilon = 1/n \ll 1$. Coordinate transformation from local to global coordinates is defined by the following tensor: $\lambda_{ij} = \cos(X_i, x_j)$ (Sokolnikoff, 1956).

2.1 Lamina Homogenization — Mori-Tanaka Model

The Mori-Tanaka model (Mori and Tanaka, 1973; Benveniste, 1987) is based on the Eshelby inclusion theory using the eigenstrains concept (Mura, 1987). The idea is to establish an average behavior defined from fiber and matrix behaviors. Hence, stress σ_{ij}, and strain e_{ij}, tensors can be defined from their average values, represented by $\langle \ldots \rangle$, evaluated on matrix and fibers (Pyrz, 2008),

$$\left\langle \sigma_{ij} \right\rangle = \frac{1}{V}\int \sigma_{ij} dv = V_f \left\langle \sigma_{ij}^{(f)} \right\rangle + (1 - V_f)\left\langle \sigma_{ij}^{(m)} \right\rangle \tag{1}$$

$$\left\langle e_{ij} \right\rangle = \frac{1}{V}\int e_{ij} dv = V_f \left\langle e_{ij}^{(f)} \right\rangle + (1 - V_f)\left\langle e_{ij}^{(m)} \right\rangle \tag{2}$$

where stresses and strains are described on local coordinate system and V_f is the fiber volume fraction.

The essential assumption for macroscopic homogenization is to establish a relationship between the average stress and the average strain tensors by equivalent stiffness tensor c_{ijkl}, allowing one to write equivalent constitutive relation $\left\langle \sigma_{ij} \right\rangle = c_{ijkl} \left\langle e_{kl} \right\rangle$. Considering that both phases are linear and elastic, it is possible to write average

equations for fibers and matrix, $\left\langle \sigma_{ij}^{(f)} \right\rangle = c_{ijkl}^{(f)} \left\langle e_{kl}^{(f)} \right\rangle$ and $\left\langle \sigma_{ij}^{(m)} \right\rangle = c_{ijkl}^{(m)} \left\langle e_{kl}^{(m)} \right\rangle$, where the stiffness tensor of both phases are known. By assuming that there is a fourth-order tensor T_{ijkl}, which relates fiber and matrix strains, $\left\langle e_{ij}^{(f)} \right\rangle = T_{ijkl} \left\langle e_{kl}^{(m)} \right\rangle$, the following expression are obtained after some tensor manipulation

$$c_{ijkl} = c_{ijkl}^{(m)} + V_f (c_{ijpq}^{(f)} - c_{ijpq}^{(m)}) T_{pqmn} [(1 - V_f) I_{mnkl} + V_f T_{mnkl}]^{-1} \tag{3}$$

Tensor T_{ijkl} can be calculated using the Eshelby inclusion principle that leads to,

$$T_{ijkl} = [I_{ijkl} - S_{ijmn} (c_{mnpq}^{(m)})^{-1} (c_{pqkl}^{(m)} - c_{pqkl}^{(f)})]^{-1} \tag{4}$$

where S_{ijkl} is the fourth-order Eshelby tensor that depends on the matrix properties and inclusion geometry shape. A set of generic solutions for isotropic and anisotropic matrix is found in Mura (1987). By considering long fibers embedded in anisotropic medium, the non-null components of this tensor are the following,

$$S_{2222} = S_{3333} = \frac{5 - 4\nu^m}{8(1 - \nu^m)} \tag{5}$$

$$S_{2233} = S_{3322} = \frac{4\nu^m - 1}{8(1 - \nu^m)} \tag{6}$$

$$S_{3311} = S_{2211} = \frac{\nu^m}{2(1 - \nu^m)} \tag{7}$$

$$S_{2323} = \frac{3 - 4\nu^m}{8(1 - \nu^m)} \tag{8}$$

$$S_{3131} = S_{1212} = \frac{1}{4} \tag{9}$$

where ν^m is the matrix Poisson's ratio.

According to Abaimov *et al.* (2016), longitudinal and transverse elastic modulus, in-plane Poisson's ratio, in-plane and out-of-plane shear modulus are computed with the following equations.

$$E_1 = V_f E_1^f + (1 - V_f) E_m + 2V_f (1 - V_f) Z_1 (\nu_{12}^f - \nu^m)^2 \tag{10}$$

$$E_2 = \frac{\dfrac{E_1}{1 - (\nu^m)^2}}{\dfrac{1}{1 - (\nu^m)^2} + 2V_f \left(\dfrac{E_1}{Z_2} \right) \left[1 + \nu_{23}^f - \dfrac{E_2^f}{E^m} (1 - \nu^m) \right] + V_f Z_1 \left(\dfrac{E_1^f}{E^m} \right) \left[\dfrac{1 + \nu^m}{E^m} - \dfrac{2}{E_1^f} + \dfrac{1 + \nu_{23}^f}{E_2^f} \right]} \tag{11}$$

$$\nu_{12} = \nu^m + 2V_f \frac{Z_1}{E^m} (\nu_{12}^f - \nu_m) [1 - (\nu^m)^2] \tag{12}$$

$$G_{12} = \frac{E^m}{2(1 - V_f)(1 + \nu^m)} \left[1 + V_f - \frac{4V_f}{1 + V_f + 2(1 - V_f) \dfrac{G_{12}^f}{E^m} (1 + \nu^m)} \right] \tag{13}$$

$$G_{23} = E^m \left\{ 2(1+\nu^m) + \frac{V_f}{\frac{1-V_f}{8[1-(\nu^m)^2]} + \frac{G_{23}^f}{E^m - 2G_{23}^f(1+\nu^m)}} \right\}^{-1} \tag{14}$$

where

$$Z_1 = \left\{ -2(1-V_f)\frac{(\nu_{23}^f)^2}{E_1^f} + (1-V_f)\frac{1-\nu_{23}^f}{E_2^f} + \frac{(1+\nu^m)[1+V_f(1-2\nu^m)]}{E^m} \right\}^{-1} \tag{15}$$

$$Z_2 = E_2^f(3+V_f-4\nu^m)(1+\nu^m) + (1-V_f)E^m(1+\nu_{23}^f) \tag{16}$$

An alternative set of equations is proposed by Liu and Huang (2014).

2.2 Lamina Strength – Bridging Model

Composite strengths can be evaluated by considering the Bridging model that can be separated into two different approaches: longitudinal and transversal. For the longitudinal strengths, where the fiber failure mechanisms are preponderant, the following equations are used (Huang and Zhou, 2011)

$$S_{11}^t = \left[V_f + (1-V_f)\left(\frac{E^m}{E_1^f}\right) \right] S_{11}^{t,f} \tag{17}$$

$$S_{11}^c = \left[V_f + (1-V_f)\left(\frac{E^m}{E_1^f}\right) \right] S_{11}^{c,f} \tag{18}$$

$$S_{12}^s = \left[V_f \frac{G_{12}^f}{(\alpha G_{12}^f + (1-\alpha)G^m)} + (1-V_f) \right] S^{s,m} \tag{19}$$

where $\alpha = 0.45$ is a reasonable value in the absence of experimental data to calibrate the model (Huang and Zhou,2011) and $S_{11}^{t,f}$ and $S_{11}^{c,f}$ are the fiber tension and compression strengths, respectively, and $S^{s,m}$ is the matrix shear strength.

On the other hand, for transverse strengths, the model assumes a matrix dominant failure and the stress concentration effect on the transverse plane. Using the Coulomb-Mohr's failure criterion, the strength predictions are given by (Huang and Xin, 2017)

$$S_{22}^t = \left[V_f \frac{E_{22}^f}{(\beta E_2^f + (1-\beta)E^m)} + (1-V_f) \right] \frac{S^{t,m}}{k_{22}^t} \tag{20}$$

$$S_{22}^c = \left[V_f \frac{E_{22}^f}{(\beta E_2^f + (1-\beta)E^m)} + (1-V_f) \right] \frac{S^{c,m}}{k_{22}^c} \tag{21}$$

$$S_{23}^s = \left[V_f \frac{E_{22}^f}{(\beta E_2^f + (1-\beta)E^m)} + (1-V_f) \right] \left(\frac{k_{22}^c}{S^{c,m}} + \frac{k_{22}^t}{S^{t,m}} \right)^{-1} \tag{22}$$

where $\beta = 0.4$ may be assumed (Huang and Zhou,2011) and $S^{t,m}$ and $S^{c,m}$ are the matrix tension and compression strengths, respectively. Additionally, based on the micromechanical point of view, the stress concentration around the fiber is given by

$$k_{22}(\varphi) = \{1 + \frac{a}{2}\sqrt{V_f}\cos(2\varphi) + \frac{b}{2(1-\sqrt{V_f})}[{V_f}^2\cos(4\varphi) + 4(1-2\cos(2\varphi))V_f\cos^2(\varphi)] + \sqrt{V_f}(2\cos(2\varphi)+\cos(4\varphi))]\}\frac{V_f E_2^f + (1-V_f)[\beta E_2^f + (1-\beta)E^m]}{\beta E_2^f + (1-\beta)E^m} \tag{23}$$

The model is completely established by defining the following parameters

$$k_{22}^t = k_{22}(0) \tag{24}$$

$$k_{22}^c = k_{22}(\phi) \tag{25}$$

$$\phi = \frac{\pi}{4} + \frac{1}{2}a\sin\left(\frac{S^{c,m} - S^{t,m}}{S^{c,m} + S^{t,m}}\right) \tag{26}$$

$$a = \frac{[1-\nu^m - 2(\nu^m)^2]E_2^f - [1-\nu_{23}^f - 2(\nu_{23}^f)^2]E^m}{(1+\nu^m)E_2^f + [1-\nu_{23}^f - 2(\nu_{23}^f)^2]E^m} \tag{27}$$

$$b = \frac{(1+\nu_{23}^f)E^m - (1+\nu^m)E_2^f}{[\nu^m + 4(\nu^m)^2 - 3]E_2^f - (1+\nu_{23}^f)E^m} \tag{28}$$

2.2 Laminate Homogenization — Asymptotic Homogenization

Once the homogenized lamina material properties are estimated, the equivalent laminate properties are computed with asymptotic homogenization (Kalamkarov and Kolpakov, 1997). Therefore, it is necessary to obtain the stiffness on the global coordinate system by the following transformation: $C_{ijkl} = \lambda_{ip}\lambda_{jq}\lambda_{kr}\lambda_{ls}c_{pqrs}$, where c_{pqrs} is the stiffness tensor on local coordinate. The equilibrium equation and the linear-elastic constitutive relation are presented in the sequence considering small displacement hypothesis and the absence of body forces,

$$\frac{\partial\sigma_{ij}^{\varepsilon}(\mathbf{X},\mathbf{y})}{\partial X_j} + \frac{1}{\varepsilon}\frac{\partial\sigma_{ij}^{\varepsilon}(\mathbf{X},\mathbf{y})}{\partial y_j} = 0 \tag{29}$$

$$\sigma_{ij}^{\varepsilon}(\mathbf{X},\mathbf{y}) = C_{ijkl}(\mathbf{y})\left[\frac{\partial u_k^{\varepsilon}(\mathbf{X},\mathbf{y})}{\partial X_l} + \frac{1}{\varepsilon}\frac{\partial u_k^{\varepsilon}(\mathbf{X},\mathbf{y})}{\partial y_l}\right] \tag{30}$$

Assuming that stress and displacement field solutions are written using a power series

$$u_i^{\varepsilon}(\mathbf{X},\mathbf{y}) = u_i^{(0)}(\mathbf{X},\mathbf{y}) + \varepsilon u_i^{(1)}(\mathbf{X},\mathbf{y}) + \varepsilon^2 u_i^{(2)}(\mathbf{X},\mathbf{y}) + \ldots \tag{31}$$

$$\sigma_{ij}^{\varepsilon}(\mathbf{X},\mathbf{y}) = \sigma_{ij}^{(0)}(\mathbf{X},\mathbf{y}) + \varepsilon\sigma_{ij}^{(1)}(\mathbf{X},\mathbf{y}) + \varepsilon^2\sigma_{ij}^{(2)}(\mathbf{X},\mathbf{y}) + \ldots \tag{32}$$

and using the stress series on equilibrium Eq.(29), the following equations are obtained matching the powers of ε on both sides (disregarding terms with powers higher than one),

$$\frac{\partial\sigma_{ij}^{(0)}(\mathbf{X},\mathbf{y})}{\partial y_j} = 0 \tag{33}$$

$$\frac{\partial\sigma_{ij}^{(0)}(\mathbf{X},\mathbf{y})}{\partial X_j} + \frac{\partial\sigma_{ij}^{(1)}(\mathbf{X},\mathbf{y})}{\partial y_j} = 0 \tag{34}$$

Now, combining the displacement and stress expansions,

$$\frac{\partial u_k^{(0)}(\mathbf{X},\mathbf{y})}{\partial y_l} = 0 \therefore u_k^{(0)}(\mathbf{X},\mathbf{y}) = u_k^{(0)}(\mathbf{X}) \tag{35}$$

$$\sigma_{ij}^{(0)}(\mathbf{X},\mathbf{y}) = C_{ijkl}(\mathbf{y})\left[\frac{\partial u_k^{(0)}(\mathbf{X})}{\partial X_l} + \frac{\partial u_k^{(1)}(\mathbf{X},\mathbf{y})}{\partial y_l}\right] \tag{36}$$

$$\sigma_{ij}^{(1)}(\mathbf{X},\mathbf{y}) = C_{ijkl}(\mathbf{y})\left[\frac{\partial u_k^{(1)}(\mathbf{X},\mathbf{y})}{\partial X_l} + \frac{\partial u_k^{(2)}(\mathbf{X},\mathbf{y})}{\partial y_l}\right] \tag{37}$$

Under these assumptions, a general periodic function on the unit cell is considered, $N_{nkl}(\mathbf{y})$, and the following relation is obtained

$$u_n^{(1)}(\mathbf{X},\mathbf{y}) = N_{nkl}(\mathbf{y})\frac{\partial u_k^{(0)}(\mathbf{X})}{\partial X_l} \tag{38}$$

Integrating Eq. (38) along the unit cell using the divergence theorem, the first-order term of the stress solution vanishes due to the unit cell equilibrium requirement (Kalamkarov and Georgiades, 2002). The zero-order stress term is the more representative, being rewritten as follows

$$\sigma_{ij}^{(0)}(\mathbf{X},\mathbf{y}) = \left[C_{ijkl}(\mathbf{y}) + C_{ijmn}(\mathbf{y})\frac{\partial N_{mkl}(\mathbf{y})}{\partial y_n}\right]\frac{\partial u_k^{(0)}(\mathbf{X})}{\partial X_l} \tag{39}$$

Integrating the other equilibrium condition

$$\frac{1}{Y}\int_Y \left[C_{ijkl}(\mathbf{y}) + C_{ijmn}(\mathbf{y})\frac{\partial N_{mkl}(\mathbf{y})}{\partial y_n}\right] d\mathbf{y}\frac{\partial^2 u_k^{(0)}(\mathbf{X})}{\partial X_j \partial X_l} = 0 \tag{40}$$

In other words, the equivalent stiffness tensor may be defined by

$$\tilde{C}_{ijkl} = \frac{1}{Y}\int_Y \left[C_{ijkl}(\mathbf{y}) + C_{ijmn}(\mathbf{y})\frac{\partial N_{mkl}(\mathbf{y})}{\partial y_n}\right] d\mathbf{y} \tag{41}$$

Considering the through thickness homogenization, a one-dimensional description is obtained and the unknown function must satisfy

$$\frac{d}{dy_3}\left[C_{i3m3}(y_3)\frac{dN_{mkl}(y_3)}{dy_3}\right] = -\frac{dC_{i3kl}(y_3)}{dy_3} \tag{42}$$

Integrating then twice along the unit cell and using the periodicity requirement to obtain the solution, the equivalent stiffness tensor is redefined as

$$\tilde{C}_{ijkl} = \left\langle C_{ijkl}\right\rangle - \left\langle C_{ijn3}C_{n3p3}^{-1}C_{p3kl}\right\rangle + \left\langle C_{ijn3}C_{n3s3}^{-1}\right\rangle\left\langle C_{s3p3}^{-1}\right\rangle^{-1}\left\langle C_{p3q3}^{-1}C_{q3kl}\right\rangle \tag{43}$$

3 MACROMECHANICS ANALYSIS

After the micromechanics analysis that defines equivalent properties obtained from the two-step homogenization, the stresses and strains distributions, as well as failure criterion are discussed on macromechanics analysis. The advantage of this multiscale approach is that it is necessary to analyze just one homogenized anisotropic tube, instead a layered tubes satisfying the equilibrium and compatibility conditions in all interfaces between plies.

3.1 Stress Distribution – Lekhnitskii Formalism

This section presents the stress solution based on Chen *et al.* (2000) and Ting (1999). Alternative derivations may be found in Lekhnitskii (1981) and Ting (1996) that employed Stroh formalism. The main idea of the methodology proposed by Chen *et al.* (2000) is that the general solution is obtained for any load combination and boundary conditions are used to determine model constants. On the other hand, the approach due to Ting (1999) needs to consider each load independently, using superposition principle in the sequence.

Consider an anisotropic tube with cylindrical anisotropy, subjected to axisymmetric mechanical loads. Moreover, assuming the generalized plane deformation hypothesis, the stress field depends only on the radial coordinate. The axisymmetric equilibrium equations are defined as follows

$$\frac{d\left\langle \sigma_{rr} \right\rangle}{dr} + \frac{\left\langle \sigma_{rr} \right\rangle - \left\langle \sigma_{\theta\theta} \right\rangle}{r} = 0 \tag{44}$$

$$\frac{d\left\langle \sigma_{r\theta} \right\rangle}{dr} + 2\frac{\left\langle \sigma_{r\theta} \right\rangle}{r} = 0 \tag{45}$$

$$\frac{d\left\langle \sigma_{rz} \right\rangle}{dr} + \frac{\left\langle \sigma_{rz} \right\rangle}{r} = 0 \tag{46}$$

Note that average values are assumed (represented by $\left\langle ... \right\rangle$) emphasizing that the macroscopic stress components are representing the homogenized cylinder. From the last two equations, it is possible to conclude that

$$\left\langle \sigma_{r\theta} \right\rangle = \frac{a_1}{r^2} \tag{47}$$

$$\left\langle \sigma_{rz} \right\rangle = \frac{a_2}{r} \tag{48}$$

where a_1 and a_2 are constants obtained according to the boundary conditions. Boundary conditions of a pressure vessel require no shear force on radial direction on both inner and outer surfaces. This means that $\left\langle \sigma_{r\theta} \right\rangle = \left\langle \sigma_{rz} \right\rangle = 0$ for any value of r, which implies that $a_1 = a_2 = 0$.

The classical approach uses stress functions to determine stress components (Lekhnitskii, 1981; Chen *et al.*, 2000). Alternatively, Ting (1999) assumed that strain components are axisymmetric being defined as follows,

$$\left\langle e_{zz} \right\rangle = \frac{du_z}{dz} = \xi \tag{49}$$

$$\left\langle e_{\theta\theta} \right\rangle = \frac{u_r}{r} \tag{50}$$

$$\left\langle e_{rr} \right\rangle = \frac{du_r}{dr} \tag{51}$$

$$\left\langle e_{z\theta} \right\rangle = \frac{1}{2}\frac{du_\theta}{dz} = \gamma r \tag{52}$$

$$\left\langle e_{rz} \right\rangle = \frac{1}{2}\frac{du_z}{dr} \tag{53}$$

$$\left\langle e_{r\theta} \right\rangle = \frac{1}{2}\left(\frac{du_\theta}{dr} - \frac{u_\theta}{r} \right) \tag{54}$$

where ξ and γ are constants that represent extension and rotation per length unit, respectively.

Using the constitutive relation

$$\xi = \tilde{C}^{-1}_{1111}\left\langle \sigma_{zz} \right\rangle + \tilde{C}^{-1}_{1122}\left\langle \sigma_{\theta\theta} \right\rangle + \tilde{C}^{-1}_{1133}\left\langle \sigma_{rr} \right\rangle + 2\tilde{C}^{-1}_{1112}\left\langle \sigma_{\theta z} \right\rangle \tag{55}$$

$$\gamma r = \tilde{C}^{-1}_{1211}\left\langle \sigma_{zz} \right\rangle + \tilde{C}^{-1}_{1222}\left\langle \sigma_{\theta\theta} \right\rangle + \tilde{C}^{-1}_{1233}\left\langle \sigma_{rr} \right\rangle + 2\tilde{C}^{-1}_{1212}\left\langle \sigma_{\theta z} \right\rangle \tag{56}$$

And manipulating Eq.(55), it is reached that

$$\left\langle \sigma_{zz} \right\rangle = \frac{\xi}{\tilde{C}^{-1}_{1111}} - \frac{1}{\tilde{C}^{-1}_{1111}}\left(\tilde{C}^{-1}_{1122}\left\langle \sigma_{\theta\theta} \right\rangle + \tilde{C}^{-1}_{1133}\left\langle \sigma_{rr} \right\rangle + 2\tilde{C}^{-1}_{1112}\left\langle \sigma_{\theta z} \right\rangle\right) \tag{57}$$

Replacing this result on Eq.(56),

$$\left\langle \sigma_{\theta z} \right\rangle = \frac{1}{2\beta_{1212}}\left(\gamma r - \frac{\tilde{C}^{-1}_{1211}}{\tilde{C}^{-1}_{1111}}\xi - \beta_{1222}\left\langle \sigma_{\theta\theta} \right\rangle - \beta_{1233}\left\langle \sigma_{rr} \right\rangle\right) \tag{58}$$

where $\beta_{ijkl} = \tilde{C}^{-1}_{ijkl} - (\tilde{C}^{-1}_{11ij} \,/\, \tilde{C}^{-1}_{1111})\tilde{C}^{-1}_{11kl}$. At this point, it is necessary to obtain the solution of the stress distributions $\left\langle \sigma_{\theta\theta} \right\rangle$ and $\left\langle \sigma_{rr} \right\rangle$ and constants γ and ξ. The solution of the radial normal stress proposed by Chen *et al.* (2000) is

$$\left\langle \sigma_{rr} \right\rangle = a_3 + a_4 r + a_5 r^{k-1} + a_6 r^{-k-1} \tag{59}$$

where $k = \sqrt{(\beta_{1212}\beta_{3333} - {\beta_{3312}}^2) \,/\, \beta_{1212}\beta_{2222} - {\beta_{2212}}^2}$. From the first equilibrium equation,

$$\left\langle \sigma_{\theta\theta} \right\rangle = a_3 + 2a_4 r + a_5 k r^{k-1} - a_6 k r^{-k-1} \tag{60}$$

Using the geometrical compatibility

$$a_3 = \left[\frac{\tilde{C}^{-1}_{1112}(\beta_{3312} - \beta_{2212}) - \beta_{1212}(\tilde{C}^{-1}_{1133} - \tilde{C}^{-1}_{1122})}{(\beta_{3333}\beta_{1212} - \beta^2_{3312}) - (\beta_{2222}\beta_{1212} - \beta^2_{2212})}\right]\xi \tag{61}$$

$$a_4 = \left[\frac{2\beta_{2212} - \beta_{3312}}{(\beta_{3333}\beta_{1212} - \beta^2_{3312}) - 4(\beta_{2222}\beta_{1212} - \beta^2_{2212})}\right]\gamma \tag{62}$$

Hence, at this point it is necessary to calculate four constants to obtain the complete solution of the stress distribution: γ, ξ, a_5 and a_6.

By considering that the pressure vessel is subjected to internal pressure p, the following boundary conditions related to the normal stress on the radial directions must be satisfied

$$\left\langle \sigma_{rr} \right\rangle_{r=R_i} = -p \tag{63}$$

$$\left\langle \sigma_{rr} \right\rangle_{r=R_e} = 0 \tag{64}$$

where R_i and R_e are the internal and external radius, respectively.

Manipulating Eq. (59), constants a_5 and a_6 are given by

$$a_5 = \frac{p - a_3[(R_i \,/\, R_e)^{-k-1} - 1] - a_4[(R_i \,/\, R_e)^{-k-1}R_e - R_i]}{(R_i \,/\, R_e)^{-k-1}{R_e}^{k-1} - {R_i}^{k-1}} \tag{65}$$

$$a_6 = \frac{p - a_3[(R_i \,/\, R_e)^{k-1} - 1] - a_4[(R_i \,/\, R_e)^{k-1}R_e - R_i]}{(R_i \,/\, R_e)^{k-1}{R_e}^{-k-1} - {R_i}^{-k-1}} \tag{66}$$

where a_3 and a_4 are defined by Eq.(63,64)))) as functions of γ and ξ. Hence, all stress components are defined depending on the extension and rotation per length unit.

Two additional boundary conditions are required. In this paper, three different conditions are analyzed based on Martins *et al.* (2014): restrained-ends, open-ends and closed-ends. A schematic representation of the boundary conditions is presented in Fig. 2.

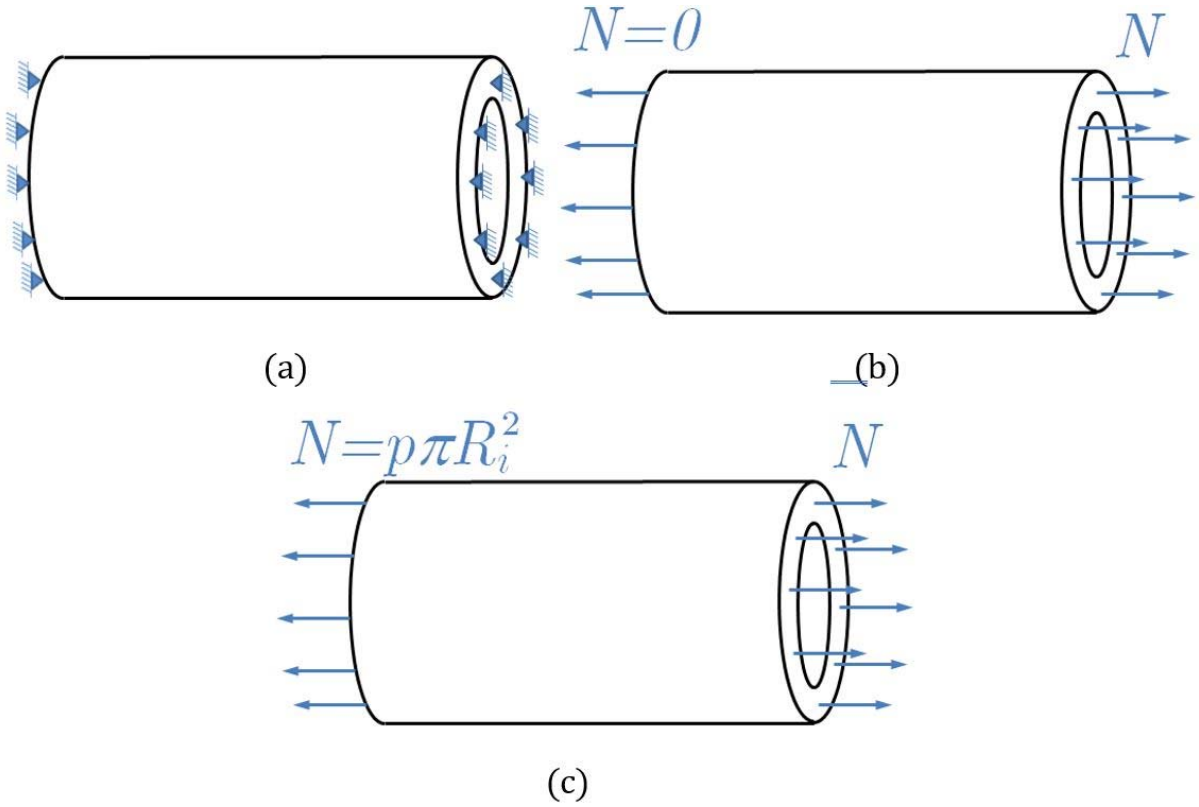

Figure 2: *Boundary conditions representation: (a) restrained-ends (plane strain); (b) open-ends; (c) closed-ends.*

Besides that, the analysis considers points far enough from the ends evoking the Saint-Venant's Principle (Sokolnikoff, 1956). For restrained-ends, plane strain condition is assumed and consequently, $\xi = \gamma = 0$. For the others, the equilibrium conditions are represented as follows

$$\int_0^{2\pi}\int_{R_i}^{R_e} \langle \sigma_{zz} \rangle r dr d\theta = N \tag{67}$$

$$\int_0^{2\pi}\int_{R_i}^{R_e} \langle \sigma_{\theta z} \rangle r^2 dr d\theta = 0 \tag{68}$$

where $N = 0$ for open-ends and $N = p\pi R_i^2$ for closed-ends. Note that, in general, the normal stress distribution is neither uniform on the cross section nor for pure axial load for anisotropic materials due to equilibrium requirements (Vignoli and Kenedi, 2016).

3.2 Failure Criterion — Tsai-Wu Model

Failure criterion is an essential issue to the composite design, allowing one to define optimum angles and maximum internal pressure. In this regard, Tsai-Wu failure criterion is employed based on the World Wide Failure Exercise (WWFE) results (Hinton *et al.*, 2004; Soden *et al.*, 2004; Kaddour and Hinton, 2013). This criterion was originally proposed as a failure criterion for any anisotropic material (Tsai and Wu, 1971; Liu and Tsai, 1998;

Kuraishi *et al.*, 2002), being not restricted to composites. Its definition is based on the following generic polynomial function of stress components,

$$f_{TW} = H_{ij}\left\langle \sigma_{ij} \right\rangle + H'_{ijkl}\left\langle \sigma_{ij} \right\rangle\left\langle \sigma_{kl} \right\rangle \tag{69}$$

where the tensor components H_{ij} and H'_{ijkl} depend on the lamina strength as well as the winding angle. Considering the strengths expressed in material coordinate, as discussed in section 2, the following tensor transformations are introduced using the tensor rotation operator:

$$H_{ij} = \lambda_{ik}\lambda_{jl}h_{kl} \tag{70}$$

$$H'_{ijkl} = \lambda_{ip}\lambda_{jq}\lambda_{kr}\lambda_{ls}h'_{pqrs} \tag{71}$$

where the non-null components of the tensors h_{kl} and h'_{pqrs} are:

$$h_{11} = \frac{1}{S_{11}^t} - \frac{1}{S_{11}^c} \tag{72}$$

$$h_{22} = h_{33} = \frac{1}{S_{22}^t} - \frac{1}{S_{22}^c} \tag{73}$$

$$h'_{1111} = \frac{1}{S_{11}^t S_{11}^c} \tag{74}$$

$$h'_{2222} = h'_{3333} = \frac{1}{S_{22}^t S_{22}^c} \tag{75}$$

$$h'_{1212} = h'_{1221} = h'_{2112} = h'_{2121} = h'_{1313} = h'_{1331} = h'_{3113} = h'_{3131} = \frac{1}{4(S_{12})^2} \tag{76}$$

$$h'_{2323} = h'_{2332} = h'_{3223} = h'_{3232} = \frac{1}{4(S_{23})^2} \tag{77}$$

$$h'_{1122} = h'_{2211} = h'_{1133} = h'_{3311} = \alpha_{12} \tag{78}$$

$$h'_{2233} = h'_{3322} = \alpha_{23} \tag{79}$$

Parameters α_{12} and α_{23} are calibration factors to represent the interaction between normal stresses. According to Liu and Tsai (1998) and Maiarú *et al.* (2017), these parameters can be expressed as follows,

$$\alpha_{12} = -\frac{1}{2\sqrt{S_{11}^t S_{11}^c S_{22}^t S_{22}^c}} \tag{80}$$

$$\alpha_{23} = -\frac{1}{2S_{22}^t S_{22}^c} \tag{81}$$

An alternative discussion about the influence of these parameters is presented by Li *et al.* (2017).
Alternatively, the failure function can be expressed in terms of strain components, given by

$$f_{TW} = H_{ij}C_{ijpq}\left\langle e_{pq} \right\rangle + H'_{ijkl}C_{ijpq}C_{klrs}\left\langle e_{pq} \right\rangle\left\langle e_{rs} \right\rangle \tag{82}$$

This approach is convenient due to three reasons: strains are continuous through the vessel's wall by compatibility conditions while the stresses are not; the effective strains obtained from the homogenized solid are similar to the actual strains on the laminate (Kalamkarov and Georgiades, 2002); the strain components in global coordinate are directly computed using the stress solution and the equivalent compliance tensor, that is obtained from the stiffness tensor in Eq. (43).

4 RESULTS

A computational implementation of the theory introduced in the previous sections is carried out. The analysis starts with a model verification establishing a comparison with some results available in literature. In this regard, it should be cited results of Christensen (2005) and Martins *et al.* (2014). Christensen (2005) discussed the classical thin-walled vessel (closed-ends condition) using the netting analysis where just tangential and longitudinal stress components are considered, assuming that only the fibers are responsible to resist the load. Martins *et al.* (2014) studied glass fiber tubes with $n = 4$, $V_f \cong 0.31$ and three different end-conditions: closed-ends, restrained-ends and open-ends. Basically, an incremental finite element analysis using shells elements is carried out, improving the capability to define end-condition requirements according to the specific geometry of the structure (a detailed discussion may be found in the reference). E-glass fibers and MY750 epoxy matrix are treated with properties presented in Table 1 and $R_i = 50.8\text{mm}$ and $t = 0.347\text{mm}$. Concerning Table 1, it should be pointed out that:

i) Glass fibers are isotropic and, to avoid loss of generality, it is employed the transversally isotropic fiber notation and therefore, it is not necessary to redefine the previously presented equations;

ii) Martins *et al*. (2014) presented mechanical properties of the lamina instead of constituent properties. They also reported that lamina tensile and compressive strength difference is around 3%, which means that they are virtually equals. Hence, it is assumed that fiber tensile and compressive strengths are equals, despite some other additional reference had obtained different values for these properties (e.g. Soden *et al*., 1998). The goal of this step is compare both results.

Table 1: *Constituent properties for model comparison (Martins et al., 2014; Soden et al., 1998).*

Glass Fiber (111A Type 30)						
E_1^f [GPa]	E_2^f [GPa]	G_{12}^f [GPa]	G_{23}^f [GPa]	ν_{12}^f	$S_{11}^{t,f}$ [MPa]	$S_{11}^{c,f}$ [MPa]
74	74	30.8	30.8	0.2	1450	1450
Epoxy Matrix (MY 750)						
E^m [GPa]	ν^m	$S^{t,m}$ [MPa]	$S^{c,m}$ [MPa]	$S^{s,m}$ [MPa]		
3.35	0.35	80	120	54		

Figure 3 presents a comparison of the proposed model and the mentioned references. The vertical red dotted line is the fiber volume fraction that Martins *et al.* (2014) carried out the analysis and the red square is the optimum angle; the blue square is the optimum condition according to the classical approach from Christensen (2005); the green line is the optimum angle variation according to the fiber volume fractions obtained using the proposed methodology and the green square is estimation for fiber volume fraction equal to those used by Martins *et al.*(2014). Considering restrained-ends, Martins *et al.* (2014) indicated that 74.5° is the optimum angle, while the present study obtained 90°, representing a difference of 20%. Nevertheless, the magnitude of the maximum pressure varies less than 4% between both results. For open-ends, Martins *et al.* (2014) obtained 88° as the optimum value while 90° is obtained with the proposed model. Finally, considering closed-ends, Martins *et al.* (2014) pointed out 53.25° and Christensen's classical approach indicates 54.74°, which are in good agreement with the result of the proposed model: 56°. Comparing the pressure magnitudes, Martins *et al.* (2014) obtained the following maximum values: 21.1 MPa for restrained-ends, 20.79 MPa for open-ends and 13.41 MPa for closed-ends; with the proposed model, the maximum pressure are 23.7 MPa for restrained-ends, 26.5 MPa for open-ends and 11.2 MPa for closed-ends. In general, it is noticeable a good agreement among the different procedures, as summarized in Table 2, since the failure criteria employed are not the same. It should be pointed out that the analytical model proposed has the advantage that the variation of the optimum angle according to the fiber volume fraction is easily computed. Note that just initial damage (FPF) is considered.

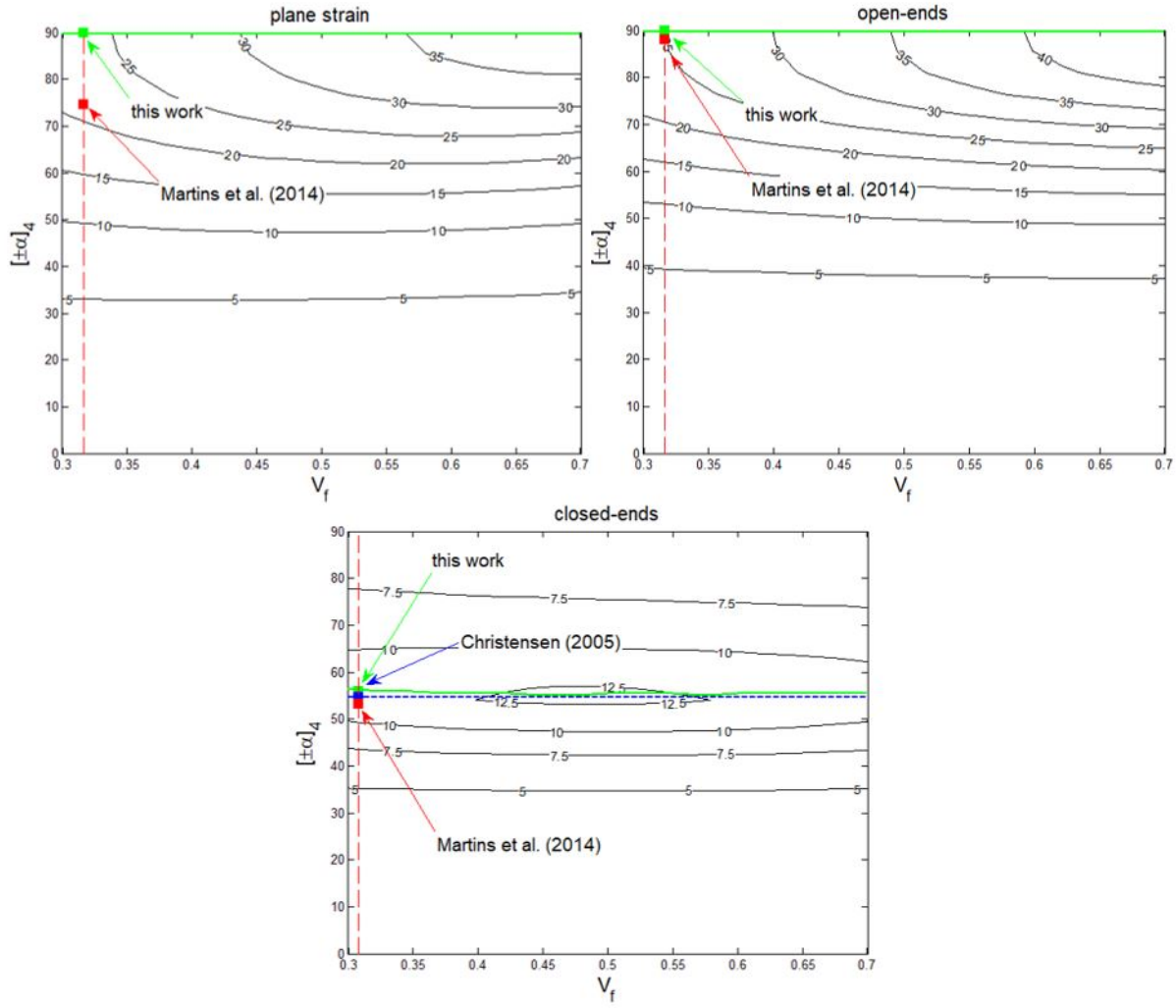

Figure 3: *Level curves of the maximum pressure: comparison of the optimum angle values obtained by Martins et al. (2014) and Christensen (2005).*

Table 2: *Summary of the optimum angle comparison.*

	This work	Martins *et al.* (2014)	Christensen (2005)
plane strain (restrained-ends)	90°	74.5°	-
open-ends	90°	88°	-
closed-ends	56°	53.25°	54.74°

Table 3: *Constituent properties for parametric analysis (Kaddour and Hinton, 2012).*

Carbon Fiber (T300)						
E_1^f [GPa]	E_2^f [GPa]	G_{12}^f [GPa]	G_{23}^f [GPa]	ν_{12}^f	$S_{11}^{t,f}$ [MPa]	$S_{11}^{c,f}$ [MPa]
231	15	15	7	0.2	2500	2000
Epoxy Matrix (PR319)						
E^m [GPa]		ν^m	$S^{t,m}$ [MPa]	$S^{c,m}$ [MPa]	$S^{s,m}$ [MPa]	
0.95		0.35	70	130	41	

The influence of lamina directions (α), wall thickness and fiber volume fraction are now investigated considering different boundary conditions. Mechanical properties of the lamina constituents (fibers and matrix) are

presented in Table 3. The lay-up related to each end condition is analyzed independently, since closed, open and restrained ends are usually design requirements that are dependent of the application and the aim here is to discuss the optimization of each one. For all the cases, the ply thickness is 1mm and the inner radius of the cylinder is 100mm.

Figures 4-6 show contour maps of the maximum allowable pressure to avoid FPF, hereafter named maximum pressure, according to the fiber volume fraction and the lamina directions. Different configurations are treated considering three end-conditions and different number of plies repetition $\pm\alpha$: $n = 10$ and $n = 50$. This kind of analysis is useful to illustrate the optimum combination and its variations. Note that the closed-ends condition is more sensitive with respect to the number of plies than the other ones. Concerning the maximum pressure, open-ends condition indicates the most considerable variation of the optimum angle. By considering restrained and closed-end vessels, Fig. 4 and Fig. 6 show that $\alpha = 90°$ and $\alpha \cong 55°$, respectively, are related to the optimal angle almost independently of the vessel thickness, similar to Fig. 3. This comparison indicates that optimum angle may be defined independently of the number of plies, fiber type and volume fraction, depending just of the end-conditions. For plane strain, $\alpha = 90°$ may be understood by the additional effort resulting from the restriction of the longitudinal direction, i.e. normal force and torsion moment, to remain without out-of-plane strain. For closed-ends, $\alpha \cong 55°$ indicates that the fiber really have a main role in this vessels to resist the load, as assumed on the classical approach (Christensen, 2005). On the other hand, for open-ends an optimum angle range of 10° is realized. This end condition has the higher sensitivity according to the vessel thickness.

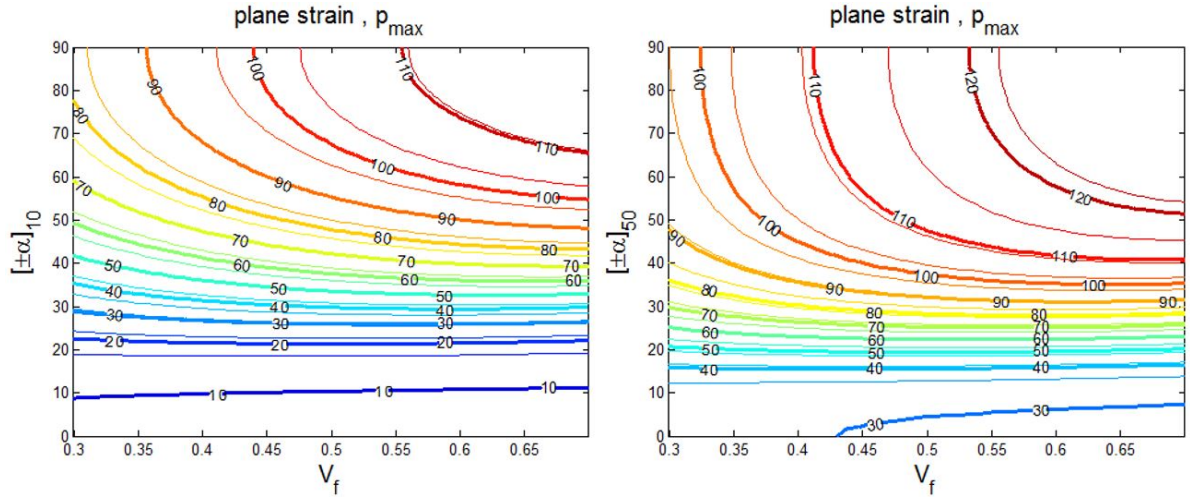

Figure 4: *Map of the maximum allowable internal pressure according to α and V_f for n = 10 and n = 50 for plane strain.*

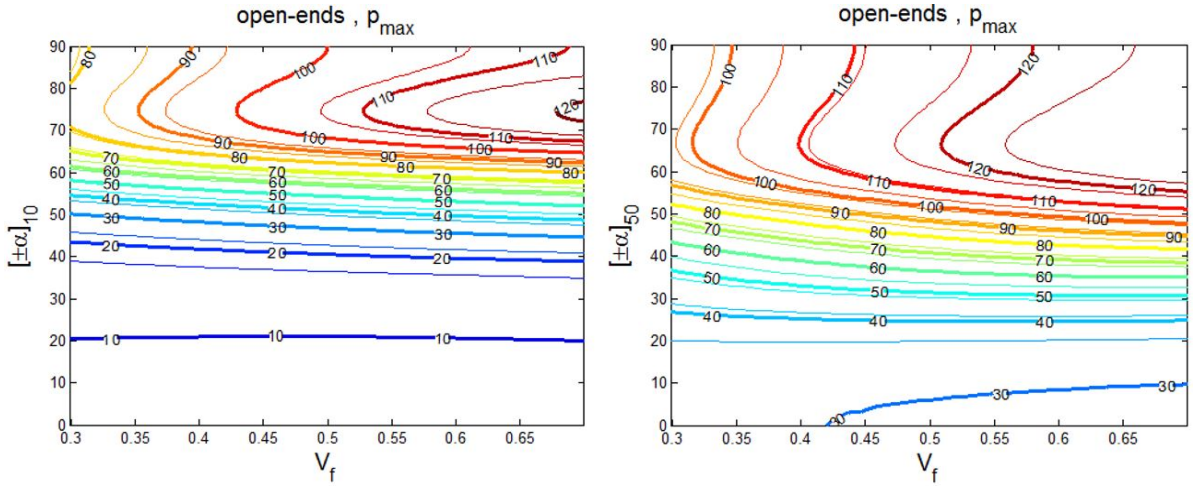

Figure 5: *Map of the maximum allowable internal pressure according to α and V_f for n = 10 and n = 50 for open-ends.*

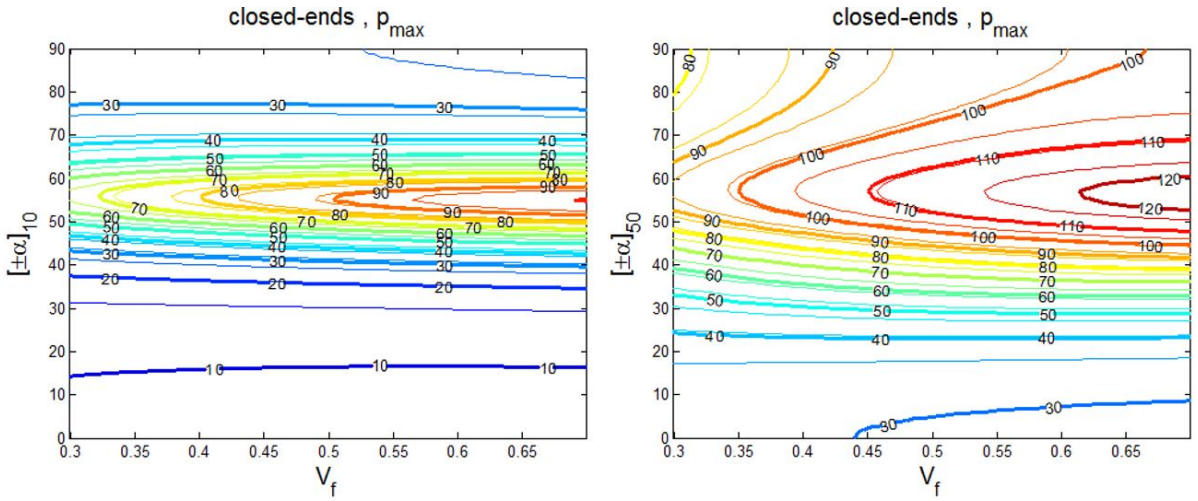

Figure 6: *Map of the maximum allowable internal pressure according to α and V_f for n = 10 and n = 50 for closed-ends.*

The increase of the number of plies may not be able to allow a considerable increase of the maximum pressure. Therefore, an alternative would be the increase of the fiber volume fraction of each ply. In order to observe this, a surface level map is presented in Fig. 7-9, where the maximum pressure is varying according to the fiber volume fraction and the number of plies. Only one angle α is chosen for each load condition (the selection is based on the optimum values presented in Fig. 4-6). An asymptotic trend of maximum pressure curves according to n is noted. In other words, the maximum pressure increases for thicker vessels and therefore, it tends to have a maximum limit, indicating that the increase of the fiber volume fraction is usually a better option than the increase the number of plies. This conclusion is only valid for FPF. An additional analysis is necessary to evaluate the influence of fiber volume fraction and number of plies in ultimate failure and the authors are not aware of this analysis available in the literature.

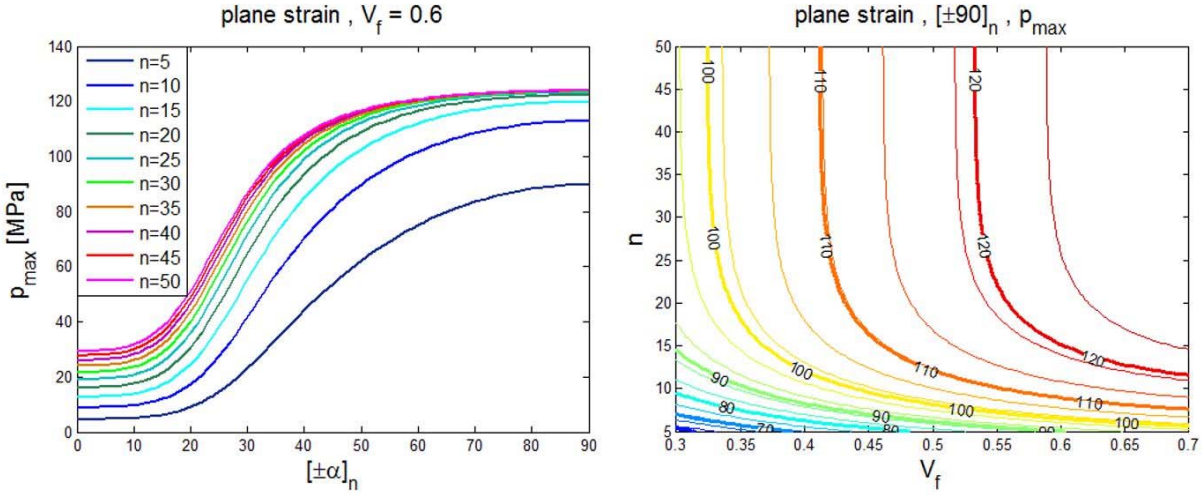

Figure 7: *Influence of the number of plies (n) on the maximum allowable internal pressure according to α (V_f = 0.6) and map of the maximum allowable internal pressure according to n and V_f for plane strain.*

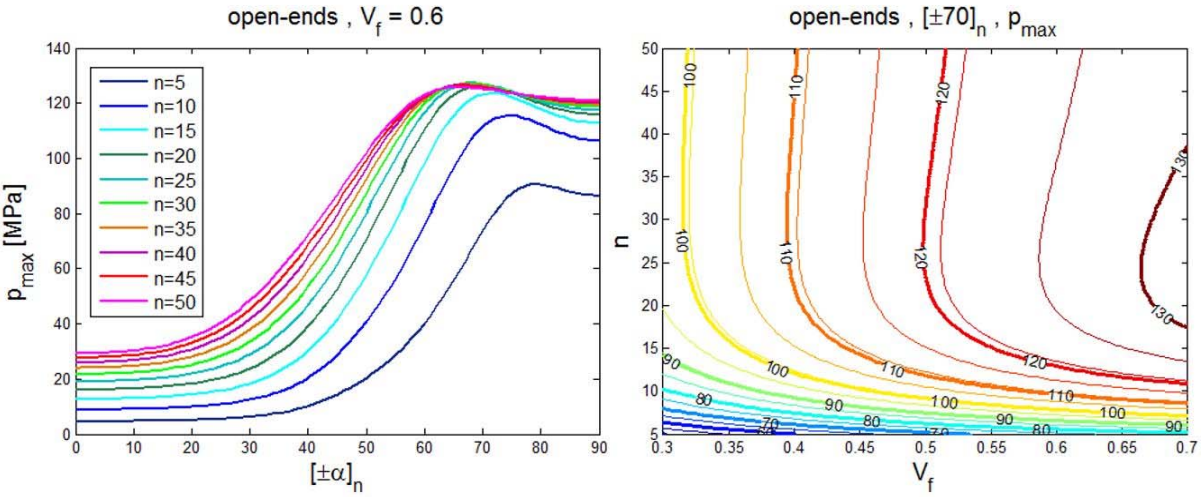

Figure 8: *Influence of the number of plies (n) on the maximum allowable internal pressure according to α (V_f = 0.6) and map of the maximum allowable internal pressure according to n and V_f for open-ends.*

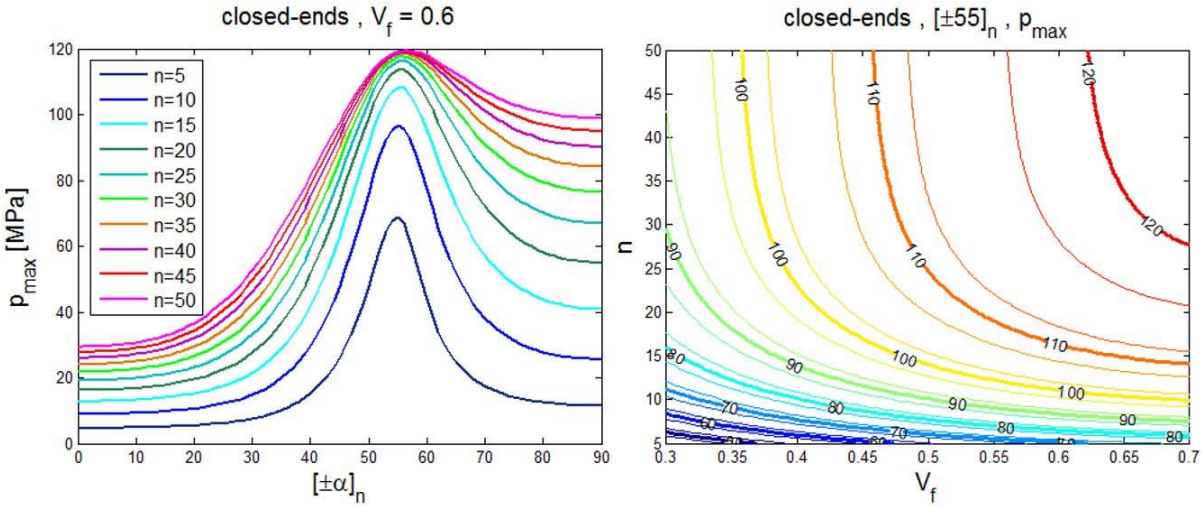

Figure 9: *Influence of the number of plies (n) on the maximum allowable internal pressure according to α (V_f = 0.6) and map of the maximum allowable internal pressure according to n and V_f for close-ends.*

4 CONCLUSIONS

This contribution presents a multiscale analytical modeling for composite pressure vessel. Micromechanics analysis is developed to define lamina equivalent properties from fiber and matrix properties; next the laminate lay-up is transformed into a homogenized anisotropic three-dimensional cylinder. Afterward, a macromechanics analysis is treated to obtain the stress-strain distribution and failure criterion. Tsai-Wu failure criterion is employed to define the maximum admissible load condition based on the elasticity solution using the Lekhnitskii formalism. Different boundary conditions are treated: open, closed and restrained ends conditions. For open-ends, neither axial force nor torsion moment are considered, while for closed-ends, the equilibrium requirement is assumed by the pressure load on the vessel end. For restrained-ends, the plane strain condition is assumed. Results are compared with other approaches available in literature showing coherent agreement. Based on the developed analysis, it is noticeable that the increase of the fiber volume fraction is a more effective approach to increase allowable pressure than the increase of the number of plies for FPF design guidelines. This conclusion may be pointed out from certain vessel thickness, for very thin vessels a considerable strength is obtained increasing the amount of layers. For angle-ply vessels, the optimum angles are close to 70° (open-ends), 55° (closed-ends) and 90° (restrained-ends or plane strain), being the open-ends vessel the most sensitive to the

number of plies. For open-ends, the optimum angle for thinner vessels tends to be closer to 80°. While the wall thickness is increasing, the angle becomes closer to 60°.

5 ACKNOWLEDGEMENTS

The authors would like to acknowledge the support of the Brazilian Research Agencies CNPq, CAPES and FAPERJ. The Air Force Office of Scientific Research (AFOSR) is also acknowledged.

References

Abaimov, S.G., Khudyakova, A.A., Lomov, S.V., (2016). On the closed form expression of the Mori–Tanaka theory prediction for the engineering constants of a unidirectional fiber-reinforced ply, Composite Structures 142, 1–6.

Almeida Jr., J.H.S, Ribeiro, M.L., Tita, V., Amico, S.C., (2016). Damage and failure in carbon/epoxy filament wound composite tubes under external pressure: Experimental and numerical approaches, Materials and Design 96, 431–438.

Ansari, R., Alisafaei, F., Ghaedi, P., (2010). Dynamic analysis of multi-layered filament-wound composite pipes subjected to cyclic internal pressure and cyclic temperature, Composite Structures 92, 1100–1109.

Barbero, E.J., (1998). Introduction to Composite Materials Design, Taylor & Francis (Philadelphia).

Benveniste, Y., (1987). A new approach to the application of Mori–Tanaka's theory in composite materials. Mech Mater 6, 147–57.

Carneiro, C.A.V., Savi, M.A., (2000). Modelling and Simulation of the delamination in composite materials, Journal of Strain Analysis, London 35, 479-492.

Carrere, N., Laurin, F., Maire, J.F., (2012a). Micromechanical-based hybrid mesoscopic 3D approach for non-linear progressive failure analysis of composite structures, Journal of Composite Materials 46, 2389–2415.

Carrere, N., Laurin, F., Maire, J.F., (2012b). Micromechanical-based hybrid mesoscopic 3D approach for non-linear progressive failure analysis of composite structures - Part B: Comparison with experimental data, Journal of Composite Materials 47, 743–762.

Chang, R.R., (2000). Experimental and theoretical analyses of first-ply failure of laminated composite pressure vessels, Technical note, Composite Structures 49, 237–243.

Chatzigeorgiou, G., Charalambakis, N., Murat, F., (2008). Homogenization problems of a hollow cylinder made of elastic materials with discontinuous properties, International Journal of Solids and Structures 45, 5165–5180.

Chen, T., Chung, C.T., Lin, W.L., (2000). A revisit of a cylindrically anisotropic tube subjected to pressuring, shearing, torsion, extension and a uniform temperature change, International Journal of Solids and Structures 37, 5143–5159.

Christensen, R.M., (2005). Mechanics of Composite Materials, Dover Publications (New York).

Cohena, D., Mantellb, S.C., Zhaob, L., (2001). The effect of fiber volume fraction on filament wound composite pressure vessel strength, Composites Part B: Engineering 32, 413–429.

Drozdov, A.D., Kalamkarov, A.L., (1995). Optimization of winding process for composite pressure vessels, International Journal of Pressure Vessel & Piping 62, 69-81.

Evans, J.T., Gibson, A.G., (2002). Composite angle ply laminates and netting analysis, Proc. R. Soc. Lond. A 458, 3079–3088.

Hinton, M.J., Kaddour, A.S., Soden, P.D., (Editors), (2004), Failure Criteria in Fibre Reinforced Polymer Composites: The World-Wide Failure Exercise, Elsevier.

Huang, Z.M. (2000). A unified micromechanical model for the mechanical properties of two constituent composite materials, Part I: Elastic behavior. J. Thermoplastic Comp. Mater. 13, 252-271.

Huang, Z.M., Xin, L.M., (2017). In situ strengths of matrix in a composite, Acta Mech. Sin. 33, 120–131.

Huang, Z.M., Zhou,Y.X., (2011). Strength of Fibrous Composites. Zhejiang University Press & Springer (Hangzhou, New York).

Kaddour, A.S., Hinton, M.J., (2012). Input data for test cases used in benchmarking triaxial failure theories of composites, Journal of Composite Materials 46, 2295–2312.

Kaddour, A.S., Hinton, M.J., (2013), Maturity of 3D failure criteria for fibre reinforced composites: Comparison between theories and experiments: Part B of WWFE-II, J. Compos. Mater. 47, 925–966.

Kalamkarov, A.L., Georgiades, A., (2002). Modeling of smart composites on account of actuation, thermal conductivity and hygroscopic absorption, Comp. B: Eng. 33, 141–152.

Kalamkarov, A.L., Kolpakov, A.G., (1997). Analysis, Design and Optimization of Composite Structures, 2nd edition, Wiley.

Kam, T.Y., Liu, Y.W., Lee, E.T., (1997). First-ply failure strength of laminated composite pressure vessels, Composite Structures 38, 65-70.

Krikanov, A.A., (2000), Composite pressure vessels with higher stiffness, Composite Structures 48, 119–127.

Kuraishi, A., Tsai, S.W., Liu, K.S., (2002). A progressive quadratic failure criterion, part B, Composites Science and Technology 62, 1683–1695.

Lekhnitskii, S.G., (1981). Theory of Elasticity of an Anisotropic Body, Mir Publishers (Moscow).

Li, S., Sitnikova, E., Liang, Y., Kaddour, A.S., (2017). The Tsai-Wu failure criterion rationalised in the context of UD composites, Composites: Part A 102, 207-217.

Liu, P.F., Chu, J.K., Hou, S.J., Zheng, J.Y., (2012). Micromechanical damage modeling and multiscale progressive failure analysis of composite pressure vessel, Computational Materials Science 60, 137–148.

Liu, K.S., Tsai, S.W., (1998). A progressive quadratic failure criterion for a laminate, Compos. Sci. Technol., 58, 1023–1032.

Liu, L., Huang, Z., (2014). A Note on Mori-Tanaka's Method, Acta Mechanica Solida Sinica 27, 234-244.

Macedo, R.Q., Ferreira, R.T.L., Guedes, J.M., Donadon, M.V., (2017). Intraply failure criterion for unidirectional fiber reinforced composites by means of asymptotic homogenization, Composite Structures 159, 335–349.

Maiarú, M., Petrolo, M., Carrera, E., (2017). Evaluation of energy and failure parameters in composite structures via a Component-Wise approach, Composites Part B 108, 53-64.

Martins, L.A.L., Bastian, F.L., Netto, T.A., (2012). Structural and functional failure pressure of filament wound composite tubes, Materials and Design 36, 779–787.

Martins, L.A.L., Bastian, F.L., Netto, T.A., (2013). The effect of stress ratio on the fracture morphology of filament wound composite tubes, Materials and Design 49, 471–484.

Martins, L.A.L., Bastian, F.L., Netto, T.A., (2014). Reviewing some design issues for filament wound composite tubes, Materials and Design 55, 242–249.

Mori, T., Tanaka, K., (1973). Average stress in matrix and average elastic energy of materials with misfitting inclusions. Acta Metall 21, 571–574.

Mura, T., (1987). Micromechanics of defects in solids. Martinus Nijhoff.

Onder, A., Sayman, O., Dogan, T., Tarakcioglu, N., (2009). Burst failure load of composite pressure vessels, Composite Structures 89, 159–166.

Parnas, L., Katırcı, N., (2002). Design of fiber-reinforced composite pressure vessels under various loading conditions, Composite Structures 58, 83–95.

Pyrz, N., (2008). Micromechanics of composites, in Lecture Notes on Composite Materials - Current Topics and Achievements, R. Borst and T. Sadowski (Editors), Springer.

Quaresimin, M., Carraro, P.A., (2014). Damage initiation and evolution in glass/epoxy tubes subjected to combined tension–torsion fatigue loading, International Journal of Fatigue 63, 25–35.

Rafiee, R., Amini, A., (2015). Modeling and experimental evaluation of functional failure pressures in glass fiber reinforced polyester pipes, Computational Materials Science 96, 579–588.

Sarvestani, H.Y., Hoa, S.V., Hojjati, M., (2016). Effects of shear loading on stress distributions at sections in thick composite tubes, Composite Structures 140, 433–445.

Sevostianov, I., Rodriguez-Ramos, R., Guinovart-Diaz, R., Bravo-Castillero, J., Sabina, F.J., (2012). Connections between different models describing imperfect interfaces in periodic fiber-reinforced composites, International Journal of Solids and Structures 49, 1518–1525.

Soden, P.D., Hinton, M.J., Kaddour, A.S., (1998). Lamina properties, lay-up conxfigurations and loading conditions for a range of fibre-reinforced composites laminates. Composite Science and Technology 58, 1011–22.

Soden, P.D., Kaddour, A.S., Hinton, M.J., (2004). Recommendations for designers and researchers resulting from the world-wide failure exercise, Compos. Sci. Technol. 64, 589–604.

Sokolnikoff, I.S., (1956). Mathematical Theory of Elasticity, Second Edition, McGraw-Hill Book Company.

Sun, X.S., Tan, V.B.C., Chen, Y., Tan, L.B., Jaiman, R.K., Tay, T.E., (2014). Stress analysis of multi-layered hollow anisotropic composite cylindrical structures using the homogenization method, Acta Mech 225, 1649–1672.

Ting, T.C.T., (1996). Pressuring, shearing, torsion and extension of a circular tube or bar of cylindrically anisotropic material, Proc. Roy. Soc. Lond. 452, 2397–2421.

Ting, T.C.T., (1999). New solutions to pressuring, shearing, torsion and extension of a cylindrically anisotropic elastic circular tube or bar, Proc. Roy. Soc. Lond, 455, 3527-3542.

Tita, V., Júnior, M.F.C., Junior, E.M., (2012). Theoretical Models to Predict the Mechanical Behavior of Thick Composite Tubes, Materials Research 15, 70-80.

Tsai, S.W., Melo, J.D.D., (2014). An invariant-based theory of composites, Composites Science and Technology 100, 237–243.

Tsai, S.W., Wu, E.M., (1971). A general theory of strength for anisotropic materials, J. Compos. Mater. 1, 58–80.

Vignoli, L.L., Kenedi, P.P., (2016). Bone Anisotropy - Analytical and Finite Element Analysis, Latin American Journal of Solids and Structures 13, 51-72.

Vignoli, L.L., Savi, M.A., (2017). Analysis of Fiber Influence in Notched Composite Plate Failure. In: ASCE-EMI International Conference 2017, Rio de Janeiro.

Wang, Y.C., Huang, Z.M., (2015). A new approach to a bridging tensor. Polym. Compos. 36, 1417–1431.